Mössbauer spectroscopy study of nanosized spinel $CoFe_2O_4$ ferrite obtained during coprecipitation followed by mechanochemical treatment

Z. Ž. LAZAREVIĆ[1,*], A. MILUTINOVIĆ[1], A. UMIĆEVIĆ[2], V. N. IVANOVSKI[2], V. KOTESKI[2], Lj. ANDJELKOVIĆ[3], N. ROMČEVIĆ[1]
[1]*Institute of Physics Belgrade, University of Belgrade, 11080, Belgrade, Serbia*
[2]*Department of Nuclear and Plasma Physics, Vinča Institute of Nuclear Sciences – National Institute of the Republic of Serbia, University of Belgrade, P.O. Box 522, 11001 Belgrade, Serbia*
[3]*University of Belgrade, Institute of Chemistry, Technology and Metallurgy, Department of Chemistry, 11000 Belgrade, Serbia*

The powdery cobalt ferrite ($CoFe_2O_4$) is prepared by coprecipitation followed by mechanochemical synthesis in a planetary ball mill. Obtained nanomaterial has been studied using a variety of characterization techniques: X-ray diffraction (XRD), Raman spectroscopy, far infrared (FIR) reflectivity and attenuated total reflectance (ATR) in combination with Fourier-transform infrared (FTIR) spectroscopy in mid IR spectra. The investigated $CoFe_2O_4$ nanomaterial showed a typical XRD pattern of cubic spinel. In the Raman and IR spectra are observed all of first-order Raman and IR active modes. Weak sub-bands activated by structure disorder are seen also. Since nano-$CoFe_2O_4$ is macroscopically cubic, its main Raman and IR modes are assigned as in normal cubic spinel. Raman spectrum is fitted with 8 Lorentzian peaks. It is observed that the value of $x = 0.58$ obtained from Raman spectrum, is in good agreement with the value obtained by XRD-structural analysis (0.51). To analyze the IR spectra, we used Decoupled Plasmon - Phonon (DPP) model of the complex dielectric function. Measurement of magnetization in the range of magnetic fields $H>>Hc$ enable the calculation of the anisotropy coefficient $K_1 = 4.02 \cdot 10^5$ J cm^{-3}, which is very high in cobalt ferrite. The ^{57}Fe-Mössbauer spectrum of the $CoFe_2O_4$ sample was measured at room temperature in ± 12 mm s^{-1} Doppler velocity range. The ^{57}Fe-Mössbauer spectrum of the $CoFe_2O_4$ sample was fitted with the extended Voigt-based fitting method.

(Received October 6, 2023; accepted June 5, 2024)

Keywords: $CoFe_2O_4$, Nanoparticles, Mössbauer spectroscopy

1. Introduction

Spinel ferrites with the general formula MFe_2O_4 (where M = Co, Mg, Zn, Mn, etc.) which belong to the characteristic group of inorganic magnetic materials, have attracted a great deal of interest in view of their potential applications in various fields [1]. During the development of new technologies, spinel oxide-type materials are considered as competent materials due to their extraordinary physical, chemical, electronic, and magnetic properties [2].

The crystal structure of spinel ferrite compounds is cubic close packing of oxygen atoms with tetrahedral and octahedral sublattices, with M^{2+} and Fe^{3+} at two different crystallographic sites, tetrahedral and octahedral oxygen coordination (A and B sites, respectively). When the 8 A sites are occupied by M^{2+} cations and the 16 B sites are occupied by Fe^{3+} the structure is referred to as normal spinel. If the A sites are completely occupied by Fe^{3+} ions and B sites are randomly occupied by Fe^{3+} and metal cations M^{2+} the structure is called inverse spinel. However, most spinels have a mixed (partially inverse) spinel structure when the cation distribution is mixed and both metal and Fe^{3+} cations are present on octahedral and tetrahedral sites, and an inversion parameter is used to describe the degree of inversion [1, 3, 4].

Transition metal ferrite nanoparticles find applications in magnetic storage systems [5], as promising photocatalysts, with good absorbance of visible light (band gap in the range 1.1-2.5 eV) [6], signal processing [7], for medical application as drug delivery and hyperthermia [8-10], magnetic resonance imaging [11] and various technical applications – as photomagnetic materials, transformer cores, high definition TV deflection yokes, in telecommunication and so on. The properties of nanoferrites largely depend on the size of the nanoparticles and on the distribution of cations between the A- and B-sites [12]. The structure and size of nanoparticles are primarily influenced by the conditions of their synthesis.

In this study we are focused on $CoFe_2O_4$. Different methods are used to synthesize cobalt ferrite [13]. Quite many works are devoted to the issues of mechanochemical synthesis of ferrites; intense research has persisted in recent years. The authors of [13-15] propose to synthesize cobalt ferrite nanoparticles in two stages: coprecipitation and mechanochemical comminution of coprecipitation

precursors. $CoFe_2O_4$ is well-known soft magnetic material - with moderate saturation magnetization (M_s) at room temperature, high chemical stability, good electrical insulation and significant mechanical hardness. The saturation magnetization of $CoFe_2O_4$ nanoparticles mainly depends on the cation inversion and decreases with increasing inversion. On the other hand, it noticeably increases with increasing nanoparticle size. When nanoparticles are annealed their M_s increase with the annealing temperature, although this increases the inversion [16]. The nanoparticles sintered at temperatures ~ 1300 K have magnetization that reaches a value as in the bulk, i.e. in a single crystal [17, 18]. Otherwise, the saturation magnetization of $CoFe_2O_4$ nanoparticles is less than that of the bulk mainly due to the existence of a "dead" layer on the nanoparticle surfaces. The effect of the disordered surface layer is greater if the nanoparticles are smaller. Cobalt ferrite has been studied in detail due to its high coercivity connected with high magnetic anisotropy - almost ten times greater than for $NiFe_2O_4$, or Fe_3O_4 [19, 20]. In the case of bigger multidomain nanoparticles coercivity is relatively low and when the crystallite size is almost equal to single-domain size, the coercivity reaches its highest value. In monodomain nanoparticles, coercivity increase with size, like anisotropy, bat it greatly depends on the synthesis method, too [2].

Ferrimagnetic $CoFe_2O_4$ is in ideal case a completely inverse cubic spinel AB_2O_4. The Co^{2+} cations are residing on the B sites and Fe^{3+} cations are distributed evenly between A- and B-sites. The strongest magnetic interaction is the antiferromagnetic A–B superexchange interaction (Fe^{3+}(A) – O^{2-} – Fe^{3+}(B)), while the A–A and B–B superexchange interactions between iron ions via oxygen ions are weaker. Other possible interactions are generally considered to be the weakest. Therefore, for ideal case, two different effective hyperfine magnetic fields are expected for bulk samples, one originated from the ^{57}Fe nuclei in A-sites and one from the ^{57}Fe nuclei in B-sites. This correspond to two superimposed six-line patterns in Mössbauer spectrum (two Mössbauer subspectra) [21-23].

In practice, bulk $CoFe_2O_4$ is usually partially inverse spinel, i.e. it is common to find Co^{2+} cations on A-sites also. The notation adopted in case of distributed Co^{2+} cations on tetrahedral and octahedral sites is $(Co_{1-x}Fe_x)[Fe_{2-x}Co_x]O_4$, the round brackets refer to cations in A-sites and the square brackets refer to cations in B-sites. The index x (x, deviation from ideal inverse spinel) take value 1 for completely inverse spinel and 0 for normal spinel.

The bulk $CoFe_2O_4$ magnetic properties depend, mostly on the kind of cations in the A and B sites and how these ions are distributed among these sites [23]. Additionally, in case of nanoparticles, other factors may influence their magnetic properties (and consequently affect the shape and lines of absorption spectra) such as size, crystallinity, morphology, preparation method, state of surface of particles, surfactants, distribution of particle size, inter-particle interactions, spin disorder (spin canting), etc. [24]. The hyperfine field is typically smaller for nanoparticles than for the bulk ones due to poorer ordering of spins within the lattice [25]. The influence of various factors is an active research field and there are many open questions among the researchers.

The aim of this work is to prepare and investigate cobalt ferrite based nanoparticles and characterize their magnetic properties with the measurements of field dependent magnetization and Mössbauer spectroscopy.

2. Materials and methods

All chemicals (iron (III) chloride hexahydrate ($FeCl_3$•$6H_2O$, 98%), cobalt (II) chloride hexahydrate ($CoCl_2$•$6H_2O$, 98%), sodium hydroxide (NaOH, >97%), were obtained by Sigma-Aldrich (p.a. quality), and used without additional purification. Deionized water was used in these experiment.

The $CoFe_2O_4$ sample was synthesized by coprecipitation followed mechanochemical synthesis method. The sample was synthesized using 0.02 mol Fe^{3+} and 0.01 mol Co^{2+} chlorides as precursors by dissolving them in 50 mL of deionized water and then heating to boiling. Mechanochemical treatment was performed in a planetary ball mill (Retsch PM100CM). A hardened-steel vial (500 cm^3 volume) filled with 10 hardened-steel balls (8 mm in diameter) was used as the milling medium. The powder prepared by the coprecipitation method was ball-milled for 10 h at 500 rpm in closed hardened steel containers with a ball-to-sample mass ratio of 20:1. The angular velocities of the supporting disc and vial were 32.2 and 40.3 rad s^{-1}, respectively. The intensity of milling corresponded to an acceleration of approximately 10 times the gravitational acceleration [26, 27].

XRD patterns were collected using a Rigaku SmartLab automated powder X-ray diffractometer with Cu Kα1 (λ = 1.54059 Å) radiation. The diffraction range was 15-90º with a step of 0.01º at a scan speed of 2º min^{-1}.

Transmission electron microscopy (TEM) analysis was performed on a JEOL JEM-1400 Plus electron microscope with a voltage of 120 kV and a LaB6 filament at different magnifications appropriate for observation of aggregation details.

The micro-Raman spectrum was taken in the backscattering configuration by Jobin Yvon T64000 spectrometer, equipped with nitrogen cooled charged coupled device detector. As an excitation source we used the 532 nm line of Ti: sapphire laser, with laser power 20 mW. The measurement was performed in the spectrum range 100 cm^{-1} to 1000 cm^{-1}.

FT-IR reflectivity measurement was carried out with a BOMMEM DA-8 FIR spectrometer. A DTGS pyroelectric detector was used to cover the wave number range from 60 to 700 cm^{-1}.

Magnetic measurement was performed using a commercial Quantum Design Physical Property Measurement System (PPMS) equipped with a 9 T superconducting magnet and a vibrating sample magnetometer (VSM) option. Temperature dependence of the magnetization, M(T), was measured upon heating in

the zero-field cooled (ZFC) and the field-cooled (FC) regime at 100 Oe from 5 to 300 K. Hysteresis loop, *M*(H), was measured at 300 K in the field range ±9 T.

The ^{57}Fe-Mössbauer spectra of the $CoFe_2O_4$ samples were measured at room temperature in ~ ± 12 mm/s Doppler velocity range. The spectra were collected in standard transmission geometry in constant acceleration mode using a ^{57}Co(Rh) source. The Doppler velocity scale was calibrated by using the Mössbauer spectrum of natural iron. The spectra were fitted by the Recoil program [28]. The center shift value (CS) is quoted relative to the natural iron (CS = 0).

3. Results and discussion

X-ray diffractograms of cobalt ferrite sample obtained by coprecipitation followed by mechanochemical treatment is presented in Fig. 1.

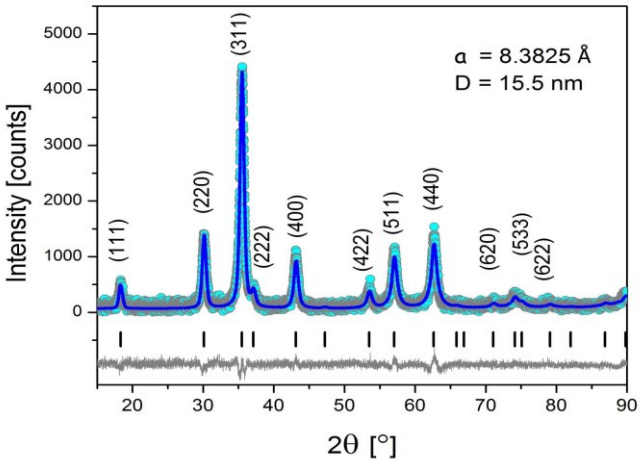

Fig. 1. X-ray diffractogram of cobalt ferrite sample obtained by coprecipitation followed by mechanochemical treatment (MC-CO) (color online)

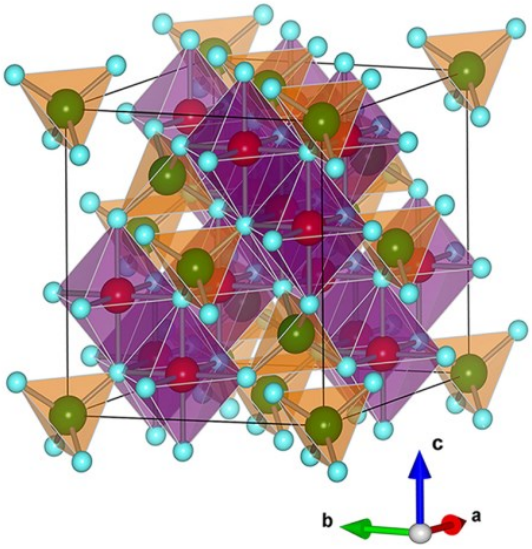

Fig. 2. Elementary spinel cubic unit cell with the space group Fd3m (origin in an occupied A-site) (color online)

It is obvious that the sample is well crystalized in single-phase spinel structure (*Fd3m* space group) with characteristic Bragg reflections indicated in figure in accordance with JCPDS PDF 22-1086. The diffractogram is analysed by means of the *FullProf Suite* [29]. A conventional elementary cubic unit cell of spinel structure with origin in an occupied A-site is presented in Fig. 2. Based on the known relations for the octahedral and/or tetrahedral distances [30], as well as the known Shannon ion radii [31] in the tetrahedral and octahedral sites, the inversion coefficient, *x*, is estimated for this sample.

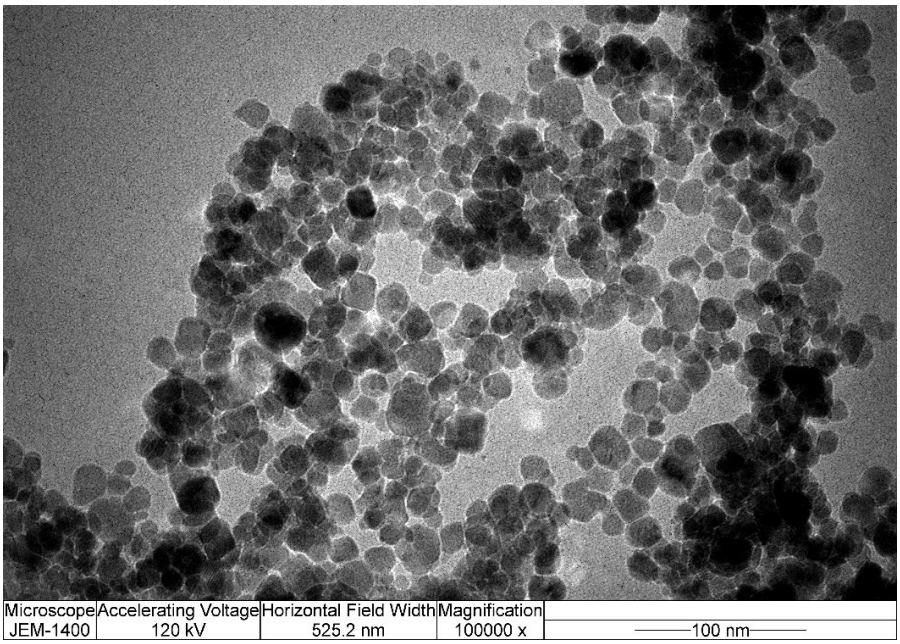

Fig. 3. TEM analysis of the synthesized cobalt ferrite

Based on the recorded TEM micrograph (Fig. 3), we were able to better analyze the microstructure of the obtained powder. The general observation is that the morphologies of the sample are not uniform, and aggregations of individual particles are the dominant process. Two kinds of particles are observed in the presented micrograph, larger polygonal and smaller particles with almost spherical shapes. The polygonal particles are larger than 20 nm, while smaller particles are in the range of 10-20 nm. The structure of smaller particles gravitates to amorphous, in contrast to polygonal ones. This could be explained by the mechanism of crystalline $CoFe_2O_4$ formation. In the first step of the chemical reaction, amorphous $CoFe_2O_4$ was formed, and, during the heat treatment, the reaction propagated along with crystallization and grain growth.

As we have already seen, the investigated $CoFe_2O_4$ sample showed a typical XRD pattern of an *Fd3m* space group, i.e. macroscopically are cubic. Raman spectra are more sensitive to local symmetry and have asymmetric or dissociated peaks characteristic for inverse and partially inverse spinel structure of lower symmetry. For the sake of simplicity (as it is usual), Raman modes are assigned as in normal cubic spinel (Fig. 4). Raman spectra are fitted with 8 Lorentzian peaks. The values of mode wave numbers are generally in accordance with literature [32, 33].

A striking feature of the cobalt ferrite Raman spectra is the separation of the A_{1g} mode in two distinct parts: $A_{1g}(1)$ corresponds to the symmetric stretching of Fe^{3+} - O bonds in tetrahedrons and $A_{1g}(2)$ to the stretching of Co^{2+} - O bonds in tetrahedrons. Weak A_{1g}* mode matches to the vibration of Fe^{3+} in incomplete tetrahedrons, as in maghemite. This specific feature of the spectra implies that the ordering of cations is much higher in tetrahedral positions than in octahedral ones.

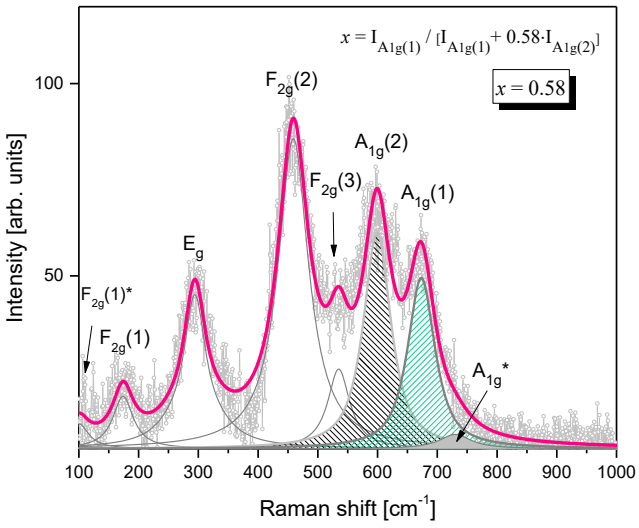

Fig. 4. Raman spectrum of cobalt ferrite with very low cation inversion $A_{1g}(2)>A_{1g}(1)$ (color online)

Consequently, due to the separation of Fe-O and Co-O oscillations, it is possible to roughly estimate the degree of inversion (xR), i.e. the Fe-content in the tetrahedral (A) estimated value of the coefficient of the inversion is given in Fig. 2. It is observed that the value of $x = 0.58$ is in good agreement with the value obtained by XRD-structural analysis.

The IR reflectivity spectrum of $CoFe_2O_4$ nanoparticle obtained by coprecipitation followed mechanochemical synthesis is shown in Fig. 5 in the range 70-700 cm^{-1}. It is clearly visible that spectra have more than four F_{1u} modes predicted by factor group analysis. All existing modes are indicated with arrows. In general, the number of vibration mode increases by canceling of degeneracy due to crystal lattice disordering, or the existence of defects and oxygen vacancies. Stretching modes of cations in a dominantly tetrahedral and octahedral environment, $F_{1u}(4)$ and $F_{1u}(3)$, respectively, are the most pronounced. It is generally accepted that the low-frequency modes $F_{1u}(2)$ and $F_{1u}(1)$ originate from complex vibrations tetrahedral and octahedral groups following with significant displacement of cations. Experimental FIR spectrum is fitted by Decoupled Plasmon - Phonon (DPP) model of the complex dielectric function $\varepsilon(\omega)$ with 5 main (+1 weak) phonon modes and a Drude therm.

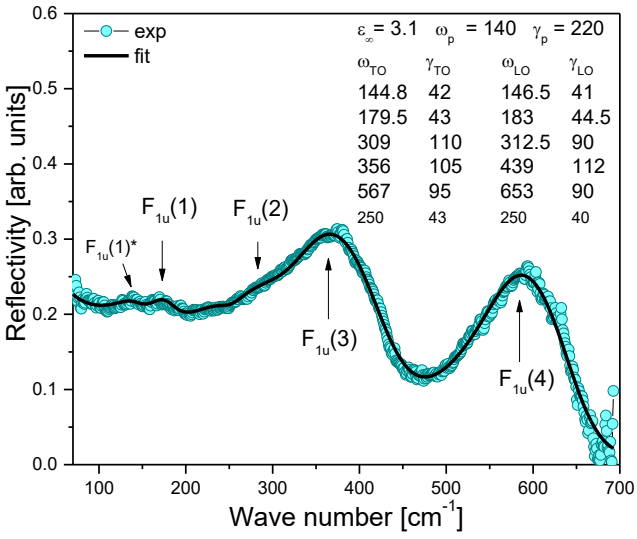

Fig. 5. FIR reflectivity spectrum of $CoFe_2O_4$ nanoparticles with parameters of the best fit (color online)

Magnetization of cobalt ferrite as the function of magnetic field is shown in Fig. 6.

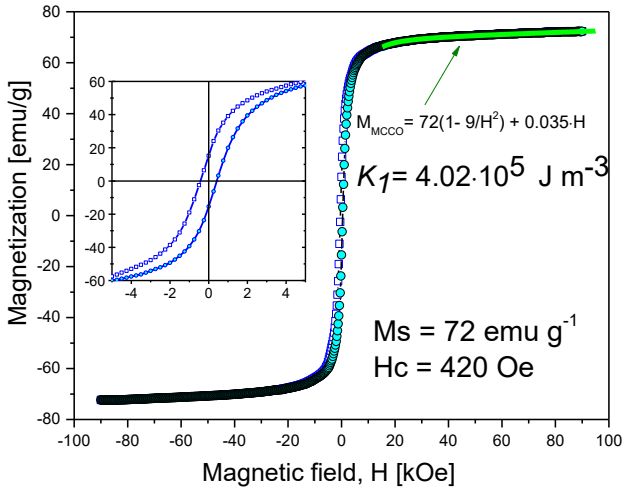

Fig. 6. Magnetization as function of magnetic field (color online)

On the graphic given in Fig. 6, green line shows a fit of M(H) for high magnetic field ($H>>Hc$) by the "low of approach to saturation". We obtain $K_1 = 4.02\cdot10^5$ [J m^{-3}] for cubic anisotropy at 300 K. The magnitude of K_1 for sintered polycrystalline cobalt ferrite is reported to vary from 2 to $4\cdot10^5$ J m^{-3}, depending upon the synthesis method [34].

The ^{57}Fe-Mössbauer spectra of the $CoFe_2O_4$ samples are presented in Fig. 7, together with the total fit. The fitted Mössbauer parameters are presented in Table 1.

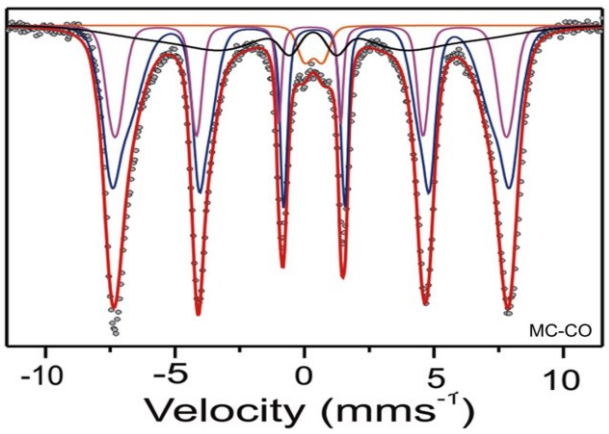

Fig. 7. Room temperature ^{57}Fe-Mössbauer spectrum of the $CoFe_2O_4$ nanoparticles sample. Experimental data are presented by the solid circles and the extended Voigt-based fit is given by the red solid line. The fitted Mössbauer sub-spectra: one doublet for superparamagnetic particles (orange), B-site (blue) sextet, A-site (dark cyan) sextet and a (black) poorly defined sextet for disturbed surface area (color online)

Table 1. The room temperature ^{57}Fe Mössbauer spectrum fitting parameters

$(Co_{1-x}\,Fe_x)^A\,[\,Fe_{2-x}\,Co_x]^BO_4$	Sub-spectra			
	QSD	HFD1 B site	HFD2 A site	HFD3
$<CS>$ [mm s^{-1}]	0.35	0.31	0.22	0.33
$<\varepsilon>$ [mm s^{-1}]		-0.064	0.02	0
$<\lvert\Delta\rvert>$ [mm s^{-1}]	0.7			
$<\lvert B_{hf}\rvert>$ [T]		45.8	46.9	35.1
St.dev.($\lvert\Delta\rvert$) [mm s^{-1}]	0.4			
St.dev.($\lvert B_{hf}\rvert$) [T]		3.6	1.8	12.8
Site Pop. [%]	3.137	55.36	23.76	17.74
x_{MOSS} PopA/PopB = x/2-x)	0.60			
x_{XRD}	0.58			

The thickness corrections were performed and the results presented are for the thin-limit spectra. The relative peak areas (3:2:1:1:2:3) and the Lorentzian linewidth (HWHM = 0.097 mm s^{-1}) were fixed during the fitting procedure. The background was not allowed to float in the fits. The minimum number of generalized sites sufficient to describe the spectra was assumed: three magnetic sites (six-line feature, sextet) and in some cases additional paramagnetic site (two-line feature, doublet). Within one generalized site, all correlations between hyperfine parameters were fixed to zero [35].

^{57}Fe-Mössbauer hyperfine parameters (Tabele 1) for the $CoFe_2O_4$ sample on room temperature are: HFD – hyperfine magnetic field distribution, QSD – qudrupole

splitting distribution; Site Pop. – site populations; <*CS*> – center shift; <|*Δ*|> – centroid (average) of quadrupole splitting distribution; st.dev.(|*Δ*|) – standard deviation of quadrupole splitting distribution (Gaussian width); <*ε*> - quadrupole shift in case of combined strong magnetic and weak electric interaction; <|B_{hf}|> – centroid (average) of hyperfine magnetic field distribution (<|B_{hf}|> for A- and B-site are effective values for multicomponent fit of hyperfine magnetic field); st.dev.(|B_{hf}|) – standard deviation of hyperfine magnetic field distribution (Gaussian width); QSD-site 1, broadened doublet; HFD-site 1, large broadened sextet B-site; HFD-site 2, broadened sextet A-site; HFD-site 3, poorly defined sextet.

The analysis of Mössbauer spectrum shows that $CoFe_2O_4$ nanomaterial has a relative small width of nanoparticle size distribution. From values of A- and B-site populations is estimated the cation inversion x_{MOSS} = 0.6 (which is in good accordance with values obtained by XRD and Raman).

4. Conclusion

Single phase cobalt ferrite $CoFe_2O_4$ was obtained by coprecipitation followed by mechanochemical treatment.

The obtained spherical monodomain nanoparticles have average size 15.5 nm and cation inversion coefficient 0.58. Based on the Raman spectra of $CoFe_2O_4$ nanomaterials, with the characteristic, fully split A_{1g} mode into components corresponding to the vibrations of different cations in the tetrahedra, the inversion coefficient of the nanomaterial was estimated. Measurement of magnetization as a function of magnetic field strength showed that $CoFe_2O_4$ nanoparticles have relatively high M_s (72 emu g^{-1} (3.03 μB)) value and characteristic K_1 ($4.02 \cdot 10^5$ J m^{-3}) anisotropy coefficient that is almost an order of magnitude higher than in other ferrites. Mössbauer spectroscopy confirms the achieved cationic inversion, a small width of the size distribution of nanoparticles and a relatively thin surface layer with a magnetically disturbed structure.

In summary, the used synthesis method resulted in a high-quality monophase nanomaterial with a narrow size distribution and low inversion coefficient, which provides it with high magnetization.

Acknowledgment

The authors acknowledge funding from the Ministry of Science, Technological Development, and Innovation of the Republic of Serbia provided by the Institute of Physics, the Vinča Institute of Nuclear Sciences (Contract No. 451-03-47/2023-01/200017) and the Institute of Chemistry, Technology and Metallurgy (Contract No. 451-03-66/2024-03/200026), University of Belgrade. This research was supported also by the Science Fund of the Republic of Serbia, Grant No. 7504386, Nano-objects in own matrix - Self composite - NOOM-Sec.

References

[1] M. P. Dojcinovic, Z. Z. Vasiljevic, V. P. Pavlovic, D. Barisic, D. Pajic, N. B. Tadic, M. V. Nikolic, J. Alloys Compd. **855**, 157429 (2021).
[2] S. M. Ansari, K. C. Ghosh, R. S. Devan, D. Sen, P. U. Sastry, Y. D. Kolekar, C. V. Ramana, ACS Omega **5**(31), 19315 (2020).
[3] C. M. B. Henderson, J. M. Charnok, D. A. Plant, J. Phys.: Condens. Matter. **19**, 076214 (2007).
[4] I. S. B. Ferraz, T. J. Castro, J. Mantilla, J. A. H. Coaquira, V. K. Garg, A. C. Oliveira, A. Franco Jr, P. C. Morais, S. W. da Silva, J. Alloys Compd. **887**, 161398 (2017).
[5] R. Sharma, P. Thakur, P. Sharma, V. Sharma, J. Alloys Compd. **704**, 7 (2017).
[6] T. Tatarchuk, M. Bououdina, J. Judith Vijaya, L. J. Kennedy, (2017). Spinel Ferrite Nanoparticles: Synthesis, Crystal Structure, Properties, and Perspective Applications, In: Fesenko, O., Yatsenko, L. (eds) Nanophysics, Nanomaterials, Interface Studies, and Applications, NANO 2016, Springer Proceedings in Physics **195**, Springer, Cham, 2016.
[7] M. Pardavi-Horvath, J. Magn. Magn. Mater. **215-216**, 171 (2000).
[8] N. Sanpo, C. C. Berndt, C. Wen, J. Wang, Acta Biomater. **9**(3), 5830 (2013).
[9] D. H. Kim, D. E. Nikles, D. T. Johnson, C. S. Brazel, J. Magn. Magn. Mater. **320**(19), 2390 (2008).
[10] M. A. Medina, G. Oza, A. Ángeles-Pascual, M. González, R. Antaño-López, A. Vera, L. Leija, Edilso Reguera, L. G. Arriaga, José Manuel Hernández Hernández, José Tapia Ramírez, Molecules **25**(19), 4428 (2020).
[11] M. Amiri, M. Salavati-Niasari, A. Akbari, Adv. Colloid. Interface Sci. **265**, 29 (2019).
[12] K. Maaz, A. Mumtaz, S. K. Hasanain, A. Ceylan, J. Magn. Magn. Mater. **308**, 28 (2007).
[13] K. O. Ptitsyna, A. A. Il'in, R. N. Rumyantsev, Yu. N. Sakharova, Glass and Ceramics **79**, 15 (2022).
[14] Y. Shi, J. Ding, H. Yin, J. Alloys Compd. **308**(1-2), 290 (2000).
[15] N. Naeinian, M. Imani, A. Tadjarodi, Materials Letters **355**, 135512 (2024).
[16] S. Briceño, W. Brämer-Escamilla, P. Silva, G. E. Delgado, E. Plaza, J. Palacios, E. Cañizales, J. Magn. Magn. Mater. **324**, 2926 (2012).
[17] A. Hussain, A. Naeem, G. Bai, Mi Yan, J. Mater. Science: Materials in Electronics **29**, 20783 (2018).
[18] M. Guillot, J. Ostorero, A. Marchand, Z. Physik B – Condensed Matter. **71**, 193 (1988).
[19] V. Blanco-Gutiérrez, M. J. Torralvo-Fernández, R. Sáez-Puche, J. Phys. Chem. C **114**(4), 1789 (2010).
[20] F. Fabris, Kun-Hua Tu, C. A. Ross, W. C. Nunes, J. Appl. Phys. **126**, 173905 (2019).
[21] G. A. Sawatzky, F. Van Der Woude, A. H. Morrish, J. App. Phys. **39**, 1204 (1968).
[22] G. A. Sawatzky, F. Van Der Woude, A. H. Morrish, Phys. Rev. **187**(2), 747 (1969).

[23] G. A. Sawatzky, F. Van Der Woude, A. H. Morrish, Phys. Rev. **183**(2), 383 (1969).
[24] X. Batlle, A. Labarta, J. Phys. D: Appl. Phys. **35**, R15 (2002).
[25] G. M. da Costa, E. De Grave, R. E. Vandenberghe, Hyperfine Interactions **117**, 207 (1998).
[26] M. Šuljagić, P. Vulić, D. Jeremić, V. Pavlović, S. Filipović, L. Kilanski, S. Lewinska, A. Slawska-Waniewska, M. R. Milenković, A. S. Nikolić, Lj. Andjelković, Mater. Res. Bull. **134**, 111117 (2021).
[27] Z. Lazarević, Lj. Andjelković, M. Šuljagić, A. Milutinović, M. Ćurčić, J. Trajić, N. Paunović, M. Romčević, B. Hadžić, N. Romčević, Optoelectron. Adv. Mat. **17**(5-6), 247 (2023).
[28] K. Lagarec, D. G. Rancourt, Recoil – Mössbauer spectral analysis software for Windows, University of Ottawa, Edition 1.0, pp. 43, 1998.
[29] J. Rodriguez-Carvajal, T. Roisnel, Full Prof. 98 and WinPLOTR: New Windows 95/NT Applications for Diffraction Commission for Powder Diffraction, International Union for Crystallography, Newletter, 20, 1998.
[30] K. E. Sickafus, J. M. Wills, N. W. Grimes, J. Am. Ceram. Soc. **82**(12), 3279 (1999).
[31] R. D. Shannon, Acta Cryst. **A32**, 751 (1976).
[32] R. S. Yadav, I. Kuřitka, J. Vilcakova, J. Havlica, J. Masilko, L. Kalina, J. Tkacz, J. Švec, V. Enev, M. Hajdúchová, Adv. Nat. Sci.: Nanosci. Nanotechnol. **8**, 045002 (2017).
[33] V. Bartunek, D. Sedmidubský, Š. Huber, M. Švecová, P. Ulbrich, O. Jankovský, Materials **11**, 1241 (2018).
[34] P. N. Anantharamaiah, P. A. Joy, Phys. Chem. Chem. Phys. **18**(15), 10516 (2016).
[35] V. Šepelák, I. Bergmann, A. Feldhoff, P. Heitjans, F. Krumeich, D. Menzel, F. J. Litterst, S. J. Campbell, K. D. Becker, J. Phys. Chem. C **111**, 5026 (2007).

*Corresponding author: lzorica@yahoo.com